M&C 2017 - International Conference on Mathematics & Computational Methods Applied to Nuclear Science & Engineering, Jeju, Korea, April 16-20, 2017, on USB (2017)

Progress in Characterizing 2D/1D Accuracy in MPACT

Michael Jarrett, Brendan Kochunas, Edward Larsen, Thomas Downar

University of Michigan, 2355 Bonisteel, Ann Arbor, MI
jarremic@umich.edu

Abstract - *The 2D/1D method is an important tool in LWR analysis that enables pin-resolved transport solutions for large, full-core simulations at relatively low computational cost compared to a true 3D transport method. To use the 2D/1D approximation, several assumptions are made about the nature of the axial (z) component of the true 3D transport solution. Generally, it is assumed that the axial variation of the solution is weak enough that the axial streaming term can be approximated as isotropic in angle, and uniform in space over a coarse pin cell, without unacceptable detriment to accuracy. Also, it is assumed that a homogenized 1D axial pin cell calculation will give the correct axial streaming magnitude and power shape. In some cases, however, we desire a more accurate transport solution; we can achieve this by implementing higher-fidelity solvers that avoid some of these coarse approximations, e.g. allowing angular dependence in the radial and axial leakage terms that couple the 2D and 1D solutions. Since the introduction of 2D/1D methods, there has been interest in developing and improving these more accurate approximations, with the ultimate goal being a 2D/1D method that limits to the 3D transport solution with spatial and angular refinement. In this paper, the 2D/1D code MPACT is used, with S_N as the 1D axial solver. We evaluate some of the approximations made in MPACT, and derive a new (to MPACT) angle-dependent 2D to 1D total cross section homogenization. The new homogenization shows good results for C5G7-type problems and the full 3D C5G7 benchmarks compared to what was previously the "most accurate" 2D/1D method in MPACT, which used angle-dependent leakages but only scalar flux homogenization of the total cross section. We also quantify the effects of applying a within-pin fine-mesh spatial shape to the axial transverse leakage, which is generally much smaller than the effect of angle-dependent homogenization.*

I. INTRODUCTION

The 2D/1D method can provide accurate solutions to 3D neutronics problems at relatively low computational cost by coupling a radial fine-mesh 2D transport solver to a coarse-mesh 1D axial solver. The 2D/1D class of methods was originally developed by two groups in Korea during 2002-2005. The "2D/1D Fusion" method, implemented in the CRX code, was developed at KAIST by N.Z. Cho, G.S. Lee, C.J. Park, and colleagues [1]. At KAERI, a slightly different method, which is simply called "2D/1D," was developed by J.Y. Cho, H.G. Joo, K.S. Kim, S.Q. Zee and colleagues. This method was implemented in DeCART [2, 3, 4, 5], and later, at SNU, in nTRACER [6].

These methods are especially useful for light water reactor (LWR) geometries, where axial heterogeneity is typically limited, and the flux variation can be separated in the radial and axial dimensions on the fine mesh, with the axial variation being well-approximated by a coarse-mesh 1D P_N or S_N solver. This approximation is the foundation of the CASL neutronics code MPACT, which is used to accurately solve large 3D LWR neutronics problems [7, 8, 9]. The 2D solver uses the Method of Characteristics (MOC) [10]. Many different 1D solvers are implemented, but the main method used for production-type analysis is P_3. In the interest of understanding and improving the accuracy of these methods, 1D axial S_N has been implemented in MPACT [11, 12] and DeCART [13].

This paper describes the main sources of error in the 2D/1D approximation. Some of these errors were rigorously quantified in previous work [5]. Some of the other errors, which are generally smaller in magnitude, have not yet been thoroughly investigated; this paper attempts to quantify these smaller errors using simple C5G7-type problems. While the standard 2D/1D method in MPACT is very similar to that in DeCART and nTRACER, this paper will focus on approximations and improvements to the higher-fidelity 2D/1D S_N solver in MPACT, which is more like the 2D/1D fusion method employed in CRX.

There are other codes that employ a similar 2D/1D concept but use different types of axial discretizations that do not require homogenization over a fuel pin cell. [14] The axial errors in these methods are fundamentally different, and are not discussed in this work. The 2D/1D error analysis in this paper applies only to codes like MPACT, DeCART, nTRACER, and CRX, which have a 2D-to-1D homogenization step.

The 2D/1D approximation in the MPACT code has been thoroughly verified and has proven to be accurate and effective for many LWR problems [9]. In general, 2D/1D accuracy is more than adequate, and the error is mostly insignificant. However, the approximation depends upon steady axial variation, and it is understood that it is somewhat less accurate near "transport boundaries" such as the tips of control rods or part-length fuel rods. While the method is generally still adequate in most cases, this presents a motivation to develop improvements that can more faithfully model these boundary layers, as well as a motivation to characterize and quantify the associated error.

Improvements to the 2D/1D method in MPACT have been studied in the past, and are still a topic of ongoing research. The thesis research of Stimpson [11] improved accuracy signif-

icantly by introducing Fourier moment expansion to increase the angular fidelity of the transverse leakages that couple the 2D and 1D solutions. Two of the potentially significant sources of error in the 2D/1D method that have not yet been addressed in MPACT are:

1. the pin-cell homogenization required for the 1D axial solver
2. the lack of a fine-mesh shape of the axial transverse leakage source in the 2D radial solver.

Both issues were briefly discussed in [11], but not addressed. In Kelley's Ph.D. thesis [15], the need for fine-mesh spatial shape was acknowledged, but again the topic was peripheral to the focus of the work and was not thoroughly studied. To the authors' knowledge, these errors have only been addressed in one other 2D/1D code: CRX. In [16], CRX is used with angle-dependent total cross section (XS) homogenization for the 1D S_N, but the discretization is too coarse (10.71 cm MOC planes, using diamond-differencing axially) to draw conclusions about the efficacy of the method. In [17], homogenization is avoided altogether by performing 1D S_N on the fine, flat-source region (FSR) mesh instead of the coarse mesh (thereby also eliminating the error due to lack of a fine-mesh distribution for the axial transverse leakage). The results were good, but computing currents on the FSR mesh boundaries is computationally impractical in most cases.

In another paper in this proceedings [18], the fine-mesh shape of the axial coupling term is investigated in a recently developed 2D/1D code, PANX. However, this code is fundamentally different from codes like MPACT, DeCART, and CRX in terms of both the transport method (variational nodal) and the axial discretization. The method lacks the homogenization step from the fine-mesh 2D to coarse-mesh 1D problem that is common to the other codes mentioned here.

In this paper, new methods are developed and implemented in MPACT that attempt to address both of these errors. As will be demonstrated, the first error (homogenization) is typically much more significant; accordingly, the focus will be on improving the 2D/1D solution through modifications to the homogenization process. Specifically, polar angle-dependent cross-section homogenization will be used so that the homogenized 1D solution more accurately reproduces the true axial power profile and streaming of the full 3D transport problem. While angle-dependent homogenization has been attempted before [16], there have never been, to the author's knowledge, thorough comparisons to standard (isotropic) homogenization that quantify the effects for typical LWR problems.

The 3D C5G7 benchmark [19] is used to evaluate the 2D/1D methods. First, the methods will be compared using a single 3D C5G7 pincell problem, followed by a partially rodded 3x3 array of UO_2 pin cells. Then, the full 3D cases of the C5G7 benchmark will be used to evaluate the effect of the homogenization error.

2D/1D is currently an important tool that the reactor physics community relies on to efficiently simulate 3D LWR neutron transport problems, including whole-core depletion and transient problems. In general, we can be relatively confident about the accuracy because of extensive verification and validation. However, we are aware that current methods have small (but non-negligible) errors when strong axial heterogeneities are present. This work represents an attempt both to understand the differences between 2D/1D and 3D transport, and to correct them.

II. THEORY

In this section we derive the 2D/1D equations to frame the discussion regarding the accuracy of the approximation. We begin with the energy-independent fixed-source 3D Boltzmann neutron transport equation with isotropic scattering:

$$\mathbf{\Omega}\cdot\nabla\psi(\mathbf{r},\mathbf{\Omega}) + \Sigma_t(\mathbf{r})\psi(\mathbf{r},\mathbf{\Omega}) = \frac{Q(\mathbf{r})}{4\pi}\ , \tag{1}$$

$$\mathbf{r} = (x,y,z)\ ,\ \Omega = \left(\sqrt{1-\mu^2}\cos\omega,\ \sqrt{1-\mu^2}\sin\omega,\mu\right)\ ,$$

$$Q(\mathbf{r}) = \left[\Sigma_s(\mathbf{r}) + \frac{\nu\Sigma_f(\mathbf{r})}{k_{eff}}\right]\int_{4\pi}\psi(\mathbf{r},\mathbf{\Omega})d\Omega\ .$$

Here, μ is the cosine of the polar angle θ, and ω is the azimuthal angle. We will derive a set of 2D transport equations and a set of 1D transport equations that is solved for each plane and pin in the problem, respectively. These equations are coupled through transverse leakage (TL) terms; the goal is to minimize the severity of the approximations made to the 3D transport equation in arriving at the 2D/1D equations.

1. 2D Equations

We first distribute the $\mathbf{\Omega}\cdot\nabla$ term from Eq. (1). Because we are not specifically interested in the radial streaming term here, we will use a shorthand notation for it:

$$(\mathbf{\Omega}\cdot\nabla)_{xy}\psi = \sqrt{1-\mu^2}\left(\cos\omega\frac{\partial}{\partial x} + \sin\omega\frac{\partial}{\partial y}\right)\psi(\mathbf{r},\mathbf{\Omega})\ , \tag{2}$$

$$(\mathbf{\Omega}\cdot\nabla)_{xy}\psi + \mu\frac{\partial\psi}{\partial z} + \Sigma_t(\mathbf{r})\psi(\mathbf{r},\mathbf{\Omega}) = \frac{Q(\mathbf{r})}{4\pi}\ . \tag{3}$$

We move the axial streaming term to the right (source) side of the equation:

$$(\mathbf{\Omega}\cdot\nabla)_{xy}\psi + \Sigma_t(\mathbf{r})\psi(\mathbf{r},\mathbf{\Omega}) = \frac{Q(\mathbf{r})}{4\pi} - \mu\frac{\partial\psi}{\partial z}\ . \tag{4}$$

The streaming term $\mu\frac{\partial\psi}{\partial z}$ is the axial TL. To obtain the 2D part of the 2D/1D equations, Eq. (4) is integrated axially over a plane, from some lower bound z^- to upper bound z^+:

$$\frac{1}{h_z}\int_{z^-}^{z^+}[Eq.\ (4)]\,dz\ ,\ h_z = z^+ - z^-\ .$$

All axial dependence is assumed to be separable from the radial and angular variables over a plane, so the axial dependence of all quantities except for the axial TL simply drops out in the integration.

$$\begin{aligned}(\mathbf{\Omega}\cdot\nabla)_{xy}\psi(x,y,\mathbf{\Omega}) + \Sigma_t(x,y)\psi(x,y,\mathbf{\Omega})\\ = \frac{Q(x,y)}{4\pi} - J_z(x,y,\mathbf{\Omega})\ ,\end{aligned} \tag{5}$$

$$J_z(x,y,\mathbf{\Omega}) = \frac{\mu}{h_z}\left[\tilde{\psi}(x,y,z^+,\mathbf{\Omega}) - \tilde{\psi}(x,y,z^-,\mathbf{\Omega})\right] . \quad (6)$$

The surface angular flux terms ($\tilde{\psi}$) are calculated in the 1D axial solver. This solution is discretized over the coarse mesh—typically one fuel pin. Thus, the axial TL term will have no fine-mesh spatial shape within a coarse cell unless we apply some shape function $g(x,y,\mathbf{\Omega})$.

$$\tilde{\psi}(x,y,z,\mathbf{\Omega}) = \hat{\psi}(z,\mathbf{\Omega})g(x,y,\mathbf{\Omega}) . \quad (7)$$

Here, $\hat{\psi}$ is the 1D axial transport solution, and $g(x,y,\mathbf{\Omega})$ is a spatial shape that we might apply, likely determined by the 2D radial solution. The fine-mesh 2D angular flux is likely the best shape function:

$$g(x,y,\mathbf{\Omega}) = \frac{\psi(x,y,\mathbf{\Omega})A_{xy}}{\int_{x^-}^{x^+}\int_{y^-}^{y^+}\psi(x,y,\mathbf{\Omega})dxdy} , \quad (8)$$

$$A_{xy} = \int_{x^-}^{x^+}\int_{y^-}^{y^+} dxdy .$$

This follows logically from Eq. (7) and the assumption of separability of the radial and axial dependence of the angular flux. However, it is prohibitively expensive to store the full angular dependence of ψ on the FSR mesh, so this information is not readily available in a typical 2D MOC calculation. We can instead take another step and assume separability between the radial (x,y) and angular variables; this leads to a scalar flux-weighted axial TL:

$$\psi(x,y,\mathbf{\Omega}) \approx \phi(x,y)f(\mathbf{\Omega}) , \quad (9)$$

$$g(x,y,\mathbf{\Omega}) = \frac{f(\mathbf{\Omega})\phi(x,y)A_{xy}}{f(\mathbf{\Omega})\int_{x^-}^{x^+}\int_{y^-}^{y^+}\phi(x,y)dxdy} ,$$

$$g(x,y) = \frac{\phi(x,y)A_{xy}}{\int_{x^-}^{x^+}\int_{y^-}^{y^+}\phi(x,y)dxdy} . \quad (10)$$

In practice, the effect of the shape function $g(x,y,\mathbf{\Omega})$ is small; in MPACT, the shape is typically ignored ($g(x,y,\mathbf{\Omega}) = 1$). We will assume $g = 1$ for now to simplify the following equations.

In MPACT, the typical approximation when using a 1D P_N method axially is to assume isotropic radial leakages. This is equivalent to operating on the right side of Eq. (5) by $\frac{1}{4\pi}\int_{4\pi}(\cdot)\,d\Omega$:

$$\left[(\mathbf{\Omega}\cdot\nabla)_{xy} + \Sigma_t(x,y)\right]\psi(x,y,\mathbf{\Omega}) = \frac{Q(x,y)}{4\pi} - \left[J(z^+) - J(z^-)\right] . \quad (11)$$

When using a P_N method of order $N > 1$, the solution $\phi_0, ..., \phi_N$ is effectively an order N Legendre expansion of $\hat{\psi}$ in μ, so we have the option of integrating only azimuthally and maintaining a polar dependence. However, the improvement is typically marginal and not worth the increased cost of storing a polar-dependent (instead of isotropic) MOC source.

When using a 1D S_N method, we know $\hat{\psi}(z^\pm,\mathbf{\Omega})$ and do not have to make any angular approximation to the axial TL. However, we can avoid significant memory requirements without appreciable loss in accuracy by expanding azimuthally in Fourier moments:

$$\hat{\psi}(z^\pm,\mu,\omega) = \hat{\psi}(z^\pm,\mu)\left(1 + \sum_{p=1}^{P}\left[A_p\sin(p\omega) + B_p\cos(p\omega)\right]\right) . \quad (12)$$

As the number of Fourier moments P increases, this representation approaches an explicit angular representation of the angular flux. As demonstrated in [11], it typically takes only $P = 2$ to get sufficiently close to the explicit angular solution.

2. 1D Equations

Now, we derive the axial 1D equations. If we swap the radial and axial streaming terms in Eq. (4), we have

$$\mu\frac{\partial\psi}{\partial z} + \Sigma_t(\mathbf{r})\psi(\mathbf{r},\mathbf{\Omega}) = \frac{Q(\mathbf{r})}{4\pi} - (\mathbf{\Omega}\cdot\nabla)_{xy}\psi(\mathbf{r},\mathbf{\Omega}) . \quad (13)$$

Next, we operate on Eq. (13) by $\frac{1}{A_{xy}}\int_{x^-}^{x^+}\int_{y^-}^{y^+}(\cdot)dxdy$. We introduce ($\hat{}$) to indicate that these variables are now discretized over a coarse cell:

$$\mu\frac{\partial\hat{\psi}}{\partial z} + \hat{\Sigma}_t\hat{\psi}(z,\mathbf{\Omega}) = \frac{\hat{Q}(z)}{4\pi} - \frac{1}{A_{xy}}\sum_{s=N,E,S,W}(\mathbf{\Omega}\cdot\hat{n}_s)\psi_s(\mathbf{\Omega}) . \quad (14)$$

The radial leakage term is summed over the 4 lateral surfaces of a rectangular coarse cell (N,E,S,W = north, east, south, and west). The surface flux $\psi_s(\mathbf{\Omega})$ is effectively a line integral over the surface s:

$$\psi_s(\mathbf{\Omega}) = \int_{u-}^{u+}\psi(u,\mathbf{\Omega})du , \quad (15)$$

where u is either x or y, depending on the surface, and the other radial variable is held constant.

Again, when the 1D solver is P_N, we operate on the right side of Eq. (14) by $\frac{1}{4\pi}\int_{4\pi}(\cdot)\,d\Omega$ to *isotropize* the radial TL, yielding

$$\mu\frac{\hat{\psi}}{dz} + \hat{\Sigma}_t\hat{\psi}(z,\mathbf{\Omega}) = \frac{1}{4\pi}\left[\hat{Q}(z) - \left(\sum_{s=N,E,S,W}J_s\right)\right] . \quad (16)$$

This is a 1D transport problem we can solve using 1D P_N. In MPACT, a nodal expansion method is used, with quadratic spatial expansion of the source and quartic expansion of the flux [20].

Alternatively, when using a 1D S_N solver, we can calculate the leakage terms explicitly (from the MOC solver) to get an anisotropic source for the S_N solver, as in Eq. (14). The surface angular flux term ψ_s can be represented by an expansion, as in Eq. (12).

Using Eqs. (5) and Eq. (14), we can accurately treat the angular dependence of the TL terms that couple the 2D and 1D solutions, leading to an improved solution compared to what can be obtained with Eqs. (11) and (16).

3. 2D to 1D Homogenization

The angle-dependent leakage terms shown in the previous section offer significant improvements in accuracy compared to isotropic leakages because they are a less severe approximation to the 3D transport equation. However, there is still an open question as to how well the radially integrated Eq. (14) will preserve physics from the 2D problem with a single, homogenized XS $\hat{\Sigma}_t$. Specifically, we want the 1D equation to preserve the average angular flux distribution over a coarse cell from the 2D problem:

$$\frac{1}{h_z}\int_{z^-}^{z^+}\hat{\psi}(z,\mathbf{\Omega})dz = \frac{1}{A_{xy}}\int_{x^-}^{x^+}\int_{y^-}^{y^+}\psi(x,y,\mathbf{\Omega})dxdy\ . \tag{17}$$

This is important because the angular flux from the 1D solution determines the axial power shape, as well as the magnitude and angular distribution of the axial TL in Eq. (6).

Typically, a standard scalar flux-weighted total XS is used:

$$\hat{\Sigma}_t = \frac{\int_{x^-}^{x^+}\int_{y^-}^{y^+}\Sigma_t(x,y)\phi(x,y)dxdy}{\int_{x^-}^{x^+}\int_{y^-}^{y^+}\phi(x,y)dxdy}\ . \tag{18}$$

Equivalently, on a discretized mesh of i fine cells with volume V_i in a coarse cell k:

$$\hat{\Sigma}_{t,k} = \frac{\sum_{i\in k}\Sigma_{t,i}\phi_i V_i}{\sum_{i\in k}\phi_i V_i}\ . \tag{19}$$

To evaluate the aptness of this definition, we will compare the 2D and 1D equations, integrated over the same cuboid volume:

$$V = \int_{x^-}^{x^+}\int_{y^-}^{y^+}\int_{z^-}^{z^+}dzdydx\ .$$

First, we integrate Eq. (5) radially $\left(\frac{1}{A_{xy}}\int_{x^-}^{x^+}\int_{y^-}^{y^+}dxdy\right)$, collecting the leakage terms on the source side:

$$\begin{aligned}&\frac{1}{A_{xy}}\int_{x^-}^{x^+}\int_{y^-}^{y^+}\Sigma_t(x,y)\psi(x,y,\mathbf{\Omega})dxdy = \\ &\frac{1}{V}\int_{x^-}^{x^+}\int_{y^-}^{y^+}\int_{z^-}^{z^+}\left(\frac{Q(\mathbf{r})}{4\pi} - (\mathbf{\Omega}\cdot\mathbf{\nabla})\psi(\mathbf{r},\mathbf{\Omega})\right)dzdxdy\ .\end{aligned} \tag{20}$$

Then, we integrate Eq. (14) axially $\left(\frac{1}{h_z}\int_{z^-}^{z^+}dz\right)$, again collecting the leakage terms on the source side:

$$\begin{aligned}&\frac{1}{h_z}\hat{\Sigma}_t\int_{z^-}^{z^+}\hat{\psi}(z,\mathbf{\Omega})dz = \\ &\frac{1}{V}\int_{x^-}^{x^+}\int_{y^-}^{y^+}\int_{z^-}^{z^+}\left(\frac{Q(\mathbf{r})}{4\pi} - (\mathbf{\Omega}\cdot\mathbf{\nabla})\psi(\mathbf{r},\mathbf{\Omega})\right)dzdxdy\end{aligned} \tag{21}$$

Because the right sides of Eqs. (20) and (21) are equivalent, we can equate the left sides. Substituting with Eq. (17), we obtain an expression for $\hat{\Sigma}_t$:

$$\hat{\Sigma}_t(\mathbf{\Omega}) = \frac{\int_{x^-}^{x^+}\int_{y^-}^{y^+}\Sigma_t(x,y)\psi(x,y,\mathbf{\Omega})dxdy}{\int_{x^-}^{x^+}\int_{y^-}^{y^+}\psi(x,y,\mathbf{\Omega})dxdy}\ . \tag{22}$$

Using Eq. (22) (or its discrete equivalent) for homogenization will give a solution $\hat{\psi}$ that satisfies Eq. (17), which should improve the accuracy of the 2D/1D solution. If we were to assume that $\psi(x,y,\mathbf{\Omega})$ is separable in space and angle, then Eq. (22) clearly reduces to Eq. (18). We can therefore infer that the severity of the error introduced by homogenizing with Eq. (18) will be directly related to the severity of the approximation of space-angle separability.

In a heterogeneous pin cell, $\psi(x,y,\mathbf{\Omega})$ is certainly not separable in space and angle. For example, when resonance or thermal energy neutrons experience a flux dip towards the center of a pin due to strong absorption and a weak source, this dip will be more severe for neutrons at steeper polar angles, which effectively have traveled a greater distance through the fuel/absorber material to get from the surface to some radial point (x,y) within a pin.

Essentially, the polar-dependent XS homogenization allows the 1D solution to account for the differences in spatial self-shielding for each of the polar angles in the quadrature set. Without angle-dependent homogenization, we are only self-shielding based on the scalar flux. This is correct for scattering or fission XS homogenization, because these sources are isotropic, so they are independent of incoming angle. Conversely, the total XS operates on the angular flux, not the scalar flux; therefore, the total XS should be homogenized with the angular flux. In the case of anisotropic scattering, the incoming angle would become a factor when homogenizing, leading to angle-dependent moments of Σ_s.

In practice, it is much easier, and likely sufficient, to use only polar-dependent total XS, because the polar dependence of the spatial self-shielding effect is much stronger than the azimuthal dependence. Effectively, this means assuming only *azimuthal* separability from the spatial-polar shape of ψ in Eq. (22), resulting in the following homogenization:

$$\hat{\Sigma}_t(\mu) = \frac{\int_{x^-}^{x^+}\int_{y^-}^{y^+}\Sigma_t(x,y)\left(\int_0^{2\pi}\psi(x,y,\mu,\omega)d\omega\right)dxdy}{\int_{x^-}^{x^+}\int_{y^-}^{y^+}\left(\int_0^{2\pi}\psi(x,y,\mu,\omega)d\omega\right)dxdy}\ . \tag{23}$$

Note that the overall zeroth angular moment neutron balance, which is satisfied by homogenizing with Eq. (18), will still be satisfied when using Eq. (22) or (23). Eq. (18) satisfies only the weak form of the balance Eq. (17), integrated over 4π, while Eq. (22) and (23) are formulated to satisfy Eq. (17) at each particular angle and each azimuthally-integrated polar angle, respectively.

The homogenization in Eq. (23) is used in this paper not just because it is simpler than Eq. (22), but also because the typical application of a 1D S_N solver in MPACT uses a moment expansion azimuthally (Eq. 12). This means that there is no discrete azimuthal angle, and no use for a discrete azimuthally dependent XS. The polar dependence of the 1D angular flux is solved independently for each Fourier moment. The polar-dependent XS is only used for the isotropic azimuthal moment; for higher moments, the isotropic XS (Eq. 18) is used.

It is possible that we could develop and implement polar-dependent XS for the higher-order azimuthal moments, but this is not done in this paper. Because the higher-order moments are often negative, the homogenization step can be complicated, and an expression like Eq. (23) would likely not work. Fortunately, the hypothetical angle-dependent XS for higher-order azimuthal moments is essentially a correction *to* a correction (to the isotropic leakage case), and the effect is probably small based on the results in this paper. At the least, it is less significant than the polar-dependent XS for the zeroth moment (azimuthally isotropic) S_N.

It is expected that the polar angle dependence of the XS will be more important than the azimuthal dependence for a few reasons. For one, the spatial self-shielding effect is more dependent on the polar angle because it directly determines how far an average neutron must travel through a pin to reach the other side. There may be an azimuthal effect for control rod neighbors, but it is likely much lower than the effect of the polar angle.

Furthermore, the azimuthally anisotropic contributions when using a moment-based 1D solver are only indirect. The 1D axial power profile is determined by the azimuthally isotropic moment. The anisotropic moments only contribute to the anisotropic moments of the axial transverse leakage; they do not change the *net* axial streaming of neutrons in the problem.

4. Summary of 2D/1D Approximations

In the previous sections we have discussed several of the approximations, and their correlated errors, that are unique to the 2D/1D equations. Of course, there are other potential sources of error that 2D/1D shares with other methods; they are not discussed in detail because they are common in neutron transport. These types of errors may include discretization error in the 2D MOC transport due to a coarse FSR mesh or ray spacing, or due to a coarse quadrature set that does not accurately model all possible directions of travel on the unit sphere. If we assume that the 2D MOC transport solution is converged in space and angle, then the remaining error in a 2D/1D solution can come from the following sources:

1. The true radial and angular shape of the angular flux is not sufficiently uniform over each plane; that is, $\psi(x, y, z, \mathbf{\Omega}) \approx \psi_z(x, y, \mathbf{\Omega}) f(z)$ is not true, because the planes are too coarse.
2. The axial variation is too strong and is not accurately captured by the chosen 1D solver—in other words, the homogenized 1D problem is not being solved accurately.
3. The angular distribution of the TL is not well-approximated by an isotropic TL term.
4. The spatial shape of the angular flux over a coarse cell is not adequately approximated by a flat axial TL.
5. The homogenized 1D problem is not a good approximation to the true heterogeneous problem because the disparity in the axial streaming *within* a coarse cell is too great for the pins to be effectively homogenized by scalar flux weighting

In MPACT, many of these errors have been addressed, or will be addressed in this paper. To briefly explain each individually:

1. This is a discretization error inherent to the 2D/1D approximation. It is corrected by axial refinement.
2. This can be (and has been) addressed by using P_3 or S_N axially, instead of diffusion.
3. Addressed in [11], where angle-dependence of the radial and axial TL terms is refined.
4. $g(x, y, \mathbf{\Omega})$ discussed in Section II.1.; thought to be small based on results in Section III
5. The main focus of this paper; shown to be a significant error in Section III, corrected by using Eq. (23) instead of Eq. (18).

These errors should be small (but not negligible) when the assumptions of 2D/1D are met, specifically the assumption that the axial variations in the solution are weak and can be accurately modeled with the chosen 1D solver and axial discretization. As long as axial variations are weak, the axial TL term should be relatively small, and the flat, isotropic approximation should not have a significant effect on the overall solution, even if it may be a poor representation of the "true" leakage.

Cases in which the assumptions are not satisfied and the errors described here may be significant are essentially what are called "transport boundary layers." These may be axial material heterogeneities (control or fuel rod tips) or axial vacuum boundaries. The goal of 2D/1D improvements is to develop better treatments to axial and radial TL or homogenization (the information by which the 2D and 1D solutions are coupled) to mitigate these errors.

Homogenization that does not accurately preserve the true physics of the 3D problem (5) can happen when there is a large disparity in the XS within a coarse pin cell. One severe example of this is an air-cooled fast reactor with a graphite-fuel matrix that has coolant channels in which axial streaming is very large. The same effect exists in LWR problems, especially in control rods, but it is less severe; thus, the error introduced from using the simpler, isotropic homogenization is generally acceptable compared to other sources of error in the model (such as the multigroup XS).

MPACT demonstrated 3D transport accuracy for problems that are piecewise homogeneous (that is, no radial heterogeneity within the pin cell coarse mesh) in [11] using 2D/1D S_N with the angular refinements developed therein. We can

infer that the remaining 2D/1D error in problems that have fine-mesh heterogeneity is a direct result of those heterogeneities; namely, errors (4) and (5) in the list. As a result, these two errors are the focus of this work.

III. RESULTS AND ANALYSIS

The results are divided into three sections. In the first section, we consider a single fuel pin cell problem. This is essentially the simplest LWR-type 3D transport problem; it allows us to quantify the effects of homogenization and spatial shape of the axial TL without confounding errors from the radial transverse leakage approximations. Next, we consider a 3x3 partially-rodded array of pins, which introduces the radial transverse leakage effect, but still avoids a global radial power tilt, which can complicate evaluations of the axial power shape. Finally, we show results for the full 3D C5G7 benchmarks to evaluate the angle-dependent homogenization method for a more realistic LWR problem. In all cases, C5G7 XS are used.

1. Single Fuel Pin Cell

The single fuel pin cell is a simple 3D transport problem that can demonstrate the errors resulting from approximations to the axial solver, such as the incorrect total XS homogenization or a spatially flat axial transverse leakage.

The problem configuration is a single UO_2 fuel pin cell with reflective boundaries on all lateral surfaces and vacuum boundaries on the top and bottom. We can change the significance of the axial streaming by making the pin shorter or longer, effectively modifying the axial buckling. If the pin is long enough, leakage has a negligible effect, and the solution is more or less the same regardless of which homogenization or leakage shape is used. As the pin becomes shorter, the leakage increases and the choice of approximation becomes important.

To evaluate the different methods, we compare the eigenvalues to a 3D multigroup Monte Carlo reference solution generated using OpenMC [21]. Each case was run using 3×10^3 inactive and 1.2×10^4 active cycles, with 2×10^4 particles per cycle (total active particles = 2.4×10^8). In MPACT, a relatively fine discretization was used, with 1.0 cm thick axial MOC planes, 144 FSRs (9 radial × 16 azimuthal), 0.01 cm ray spacing, and a Chebyshev-Gauss quadrature with 16 azimuthal and 8 polar angles per octant.

The results are shown in Fig. 1. The uncertainty is 5 pcm or lower in each case; this is not shown in the figure because it would be difficult to see on the necessary scale. "ISO XS" refers to isotropic total XS in 1D, i.e., scalar flux homogenization [Eq. (18)]. "POLAR XS" refers to polar angular flux weighted XS (Eq. 23), and "SCALAR TL" refers to scalar flux weighted axial TL leakage (Eq. 10).

When the pin is very long, the two types of homogenization converge to the same, correct answer. For shorter lengths (higher leakages), scalar flux homogenization has a large error that is corrected by polar homogenization. The polar homogenization case is within two standard deviations of the Monte Carlo eigenvalue for all pins 50 cm or greater in length, with or without scalar flux-weighted axial TL. For pins below this

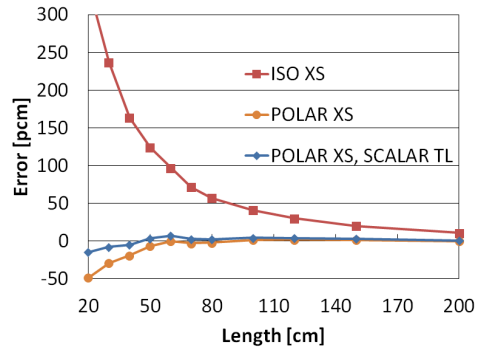

Fig. 1: 3D UO_2 pincell results

length, scalar flux-weighting of the TL appears to improve the eigenvalue, keeping it within two standard deviations down to 30 cm. However, it is worth noting that the effect of polar homogenization is more than 10 times greater than the effect of scalar flux-weighted TL.

Angular flux-weighted TL, which should be slightly better than scalar flux weighting, was not used here, or anywhere in this paper, because it caused instability due to a negative total source in nearly every case.

In this case, it appears that whatever error there may be from ignoring the azimuthal dependence in the homogenization step is negligible. This is not a surprise because azimuthal dependence should not be especially important in an infinite lattice problem. The polar-dependent homogenization gives an eigenvalue within uncertainty over a large range of pin heights, indicating that it is an important effect, which is greater in magnitude than the effect of neglecting the azimuthal angle.

The trend in Fig. 1 is more important than the actual magnitude of the errors. Obviously, LWR cores are not actually 20 cm long, so we do not see 300 pcm errors due to homogenization for real problems. However, this study highlights the critical defect in scalar flux homogenization that is present wherever axial streaming is significant. This effect is still present in very tall LWR cores–albeit on a smaller scale–near heterogeneities such as a partially-inserted control rod. We consider a simple example of this case next.

2. 3x3 Partially Rodded Lattice

For the 3x3 partially-rodded lattice problem, we use a square of UO_2 fuel pins with a guide tube in the center position. The axial length is equivalent to the 3D C5G7 benchmark (42.84 cm of fuel, 21.42 cm of moderator). The control rod is inserted from the top to the halfway point of the fuel (21.42 cm from the bottom). All lateral boundaries and the bottom are reflective; the top boundary is vacuum. The reference solution was again generated with OpenMC, using 2×10^4 particles per cycle, 5×10^3 inactive and 2×10^4 active cycles (total active particles = 4×10^8).

The radial discretization is the same as in the single pin cell problem, but the number of polar angles has been reduced from 8 per octant to 4, which is more typical of a practical case. To demonstrate that results are not confounded by discretization error, we first run with increasing numbers of Fourier moments in the radial TL and axial angular flux expansion,

from 0 to 3, and then we increase the number of the axial planes from 18 to 72.

From Fig. 2 we observe that the eigenvalue is converged at $P = 2$ (isotropic, two sine, and two cosine moments). We set $P = 2$ and then refine axially from 18 to 72 planes in Fig. 3. Here we can see that the eigenvalue does not appear to converge with increasing axial refinement; instead, it continues to get closer to the Monte Carlo reference. However, the planes could not be refined any further than 72 (0.8925 cm each). Regardless of the homogenization or axial TL shape, 2D/1D is unstable with finer planes for this problem, due to negative total sources from axial transverse leakage. Fortunately, we are already quite close to the reference solution at this plane height, and we should expect that the solution would converge soon upon additional refinement.

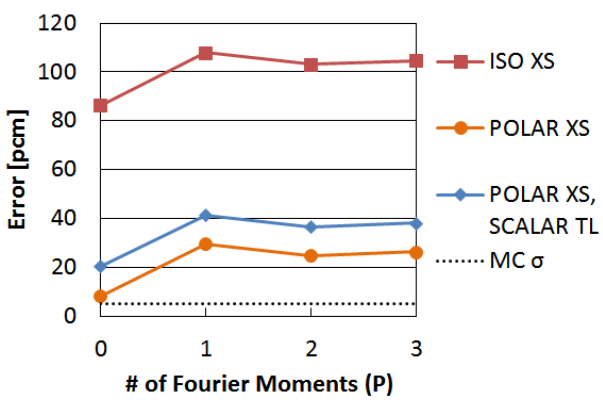

Fig. 2: Eigenvalue error for 3x3 problem, azimuthal refinement

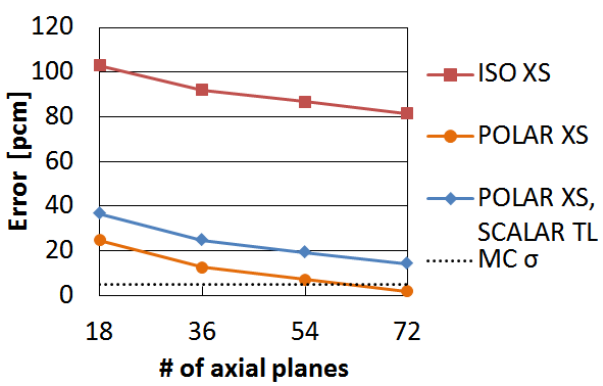

Fig. 3: Eigenvalue error for 3x3 problem, axial refinement

There is a trend in these plots similar to what was observed for the pincell problem: the eigenvalue error is significantly reduced when using polar homogenization, and the effect of the axial TL shape is about one order of magnitude smaller than the effect of polar homogenization.

Next, we consider the power errors with angle refinement in Fig. 4 and axial refinement in Fig. 5. The max errors are connected by solid lines, the RMS errors by dotted lines. Again, we find that polar homogenization reduces the error significantly, while the effect of the axial TL spatial shape is small. One noteworthy observation is that both the eigenvalue and the pin power are more accurate in the least refined case ($P = 0$, 3.57 cm planes) using polar homogenization than in the most refined case ($P = 2$, 0.8925 cm planes) using scalar flux homogenization.

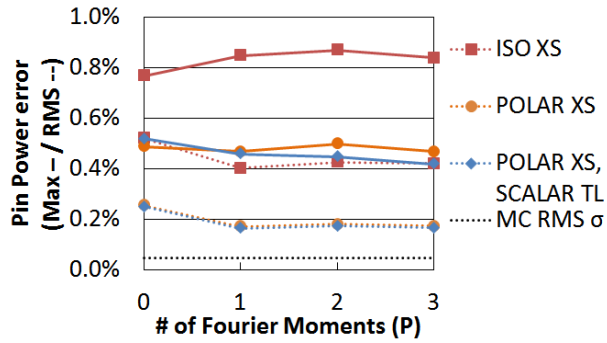

Fig. 4: Pin power error for 3x3 problem, azimuthal refinement

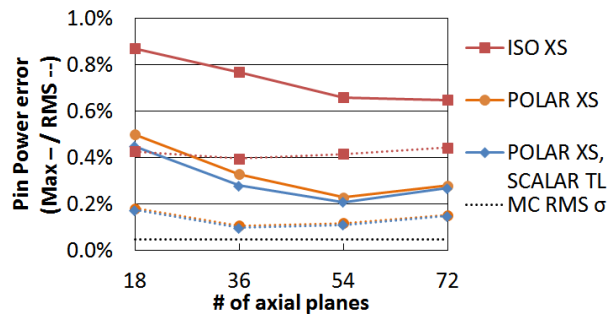

Fig. 5: Pin power error for 3x3, axial refinement

In Fig. 4 it appears that the number of azimuthal moments used in the TL leakage and 1D angular flux expansion does not have a significant effect on the pin power. This is because the azimuthal moments help resolve radial transport effects, but the main error in this case is due to an axial transport effect (the partially-inserted control rod). Increasing the number of azimuthal moments does not help 2D/1D resolve the axial transport boundary without polar XS homogenization.

To see how polar homogenization improves the pin powers, we compare the errors for the side pin in the array (the direct neighbor of the control rod) in Fig. 6.

A large error occurs at 21.42 cm using scalar flux homogenization, which is the location of the tip of the control rod. This is a strong axial heterogeneity, and the self-shielding in both the control rod and the fuel pins is important here. With polar homogenization, the pin power error at the control rod tip is much smaller. With axial TL spatial shape, the change in the pin power profile is not significant. If we could continue refining the axial planes indefinitely, the 2D/1D pin power should eventually converge to the 3D transport solution with polar homogenization. Conversely, an error occurs at the control rod tip when using scalar flux homogenization that will not be corrected with refinement.

3. 3D C5G7 Benchmark

The 3D C5G7 benchmark [19] is a common benchmark for evaluating the accuracy of neutronics codes. The geometry

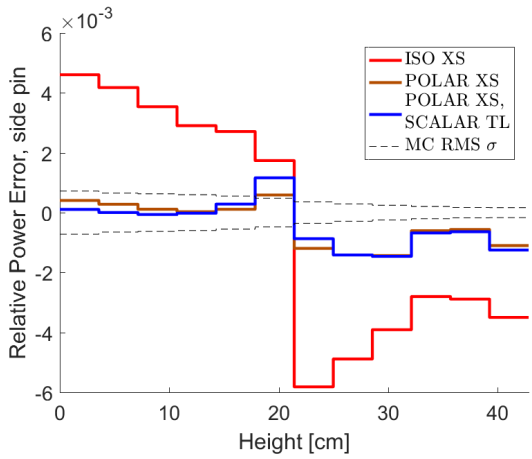

Fig. 6: Side pin power error, 3x3

is two UO_2 and two MOX fuel assemblies, arranged in a checkered pattern, with reflective boundaries on the west and south surfaces. On the other sides the core is surrounded by moderator assemblies, and on the outside of those the boundary condition is vacuum. For 3D, there are 3 standard configurations: unrodded, and two rodded cases (A and B). In the rodded A case, the rods are partially (1/3) inserted into the center UO_2 assembly. In rodded B, the rods are (1/3) inserted into both MOX assemblies, and (2/3) into the center UO_2 assembly.

The strong axial variation in the C5G7 benchmark is typically handled quite well, from the perspective of accuracy, by the 2D/1D S_N solver in MPACT. However, the strong axial TL can cause negative total sources, leading to instability. Unfortunately, there is not yet any way to resolve this instability in general cases *without* severely damaging the accuracy. The C5G7 benchmarks flirt with this line of instability, but can converge with a sufficient number of upscattering and inner transport sweeps per outer iteration.

When the polar-dependent homogenization is used, the axial TL is increased over the scalar homogenization case, which in most cases means that more transport sweeps per outer iteration are required to converge to the solution without instability. In all 3 cases here, 3 upscattering sweeps and 3 inner sweeps per group were required to achieve stability. Because the number of outer iterations required to converge is not decreased by increasing the number of transport sweeps per outer, this significantly increases the computational time required to reach convergence.

The discretization was relatively fine: 144 FSRs per pin cell (9 radial x 16 azimuthal), 225 FSRs per moderator cell (cartesian 15x15), 0.02 cm ray spacing, and 16 azimuthal $\times$ 4 polar angles per octant in the quadrature set (Chebyshev azimuthal, Gauss polar). The transverse leakage treatment was moment based ($P = 2$). The quadrature is not sufficiently refined; for example, there is a +22 pcm change in the eigenvalue for the 2D C5G7 problem if the number of angles is doubled in each dimension to 32 azimuthal $\times$ 8 polar per octant. However, increasing the number of polar angles per octant tends to cause instability for these problems, so angular refinement will be considered after potential future developments in stabilization.

The axial discretization is eighteen 3.57 planes, which is the same as the coarse case in Section III.2. In those results, we saw the eigenvalue decrease by 23 pcm as the planes were refined by a factor of 4, from 3.57 cm to 0.8925 cm. We should keep this is mind, as well as potential quadrature error, when viewing the results of the full 3D cases.

Pin power and eigenvalue results for the 3D C5G7 benchmark without and with polar-dependent XS are given in Tables I and II, respectively. With the polar-dependent XS, we see a change in eigenvalue of 15–40 pcm. The eigenvalues are not within uncertainty, but we shouldn't expect them to be when considering the likely discretization errors. The more significant result is the pin power (fission rate) errors: the RMS pin power decreases by more than 50% in all three cases, and the max pin power error decreases by 15-40%. The pin power errors are plotted in the Appendix.

TABLE I: 3D C5G7 benchmark errors, isotropic XS

	k_{eff} [pcm]	RMS [%]	Max [%]
unrodded	4	0.28	0.88
rodded A	18	0.36	1.15
rodded B	21	0.55	2.27

TABLE II: 3D C5G7 benchmark errors, polar XS

	k_{eff} [pcm]	RMS [%]	Max [%]
unrodded	-10	0.12	0.53
rodded A	-11	0.18	0.99
rodded B	-20	0.27	1.74

IV. CONCLUSIONS

In this paper, we derived an improved method for homogenizing cross sections for the 1D axial kernel of a 2D/1D solver in MPACT. This is not the first time that angle-dependent XS homogenization has been considered, but it is the first time that it has been used with the 2D/1D solver in MPACT, and these are the most complete and significant results using this method, to the author's knowledge. This method involves using polar-dependent angular flux-volume weighted homogenization of the total XS, instead of scalar flux-volume weighted homogenization. This method makes the solution of the 1D equation consistent with the 2D solution integrated over the same 3D pin cell volume for each polar angle. With scalar flux homogenization, only the zeroth angular moment (scalar) flux from the 2D equation is preserved, not the angular distribution. The 2D solution has important information about the angular distribution of the flux that is necessary for the 1D solution to model the axial streaming correctly.

We also considered the effect of the spatial distribution of the axial transverse leakage, and proposed two spatial shape functions: scalar flux weighting and polar angular flux weighting. The polar flux weighting should be more correct, but the peak spatial shape factor is much greater for the polar flux than the angular flux; this leads to very consistent instability. Using scalar flux weighting, we saw that a spatial TL shape has a relatively small eigenvalue effect (compared to polar-dependent XS), and virtually no effect on the pin power shape.

While previous work has been done to quantify the effects of larger 2D/1D errors such as using a diffusion approximation axially [5], this work quantifies some of the lesser 2D/1D errors (homogenization, spatial TL shape) that have not been studied as rigorously but are important in a highly refined regime where very good accuracy is expected.

The polar-dependent XS showed very good results for the pincell and 3x3 problems. For the full 3D C5G7 benchmark problems, there was significant improvement in every case when going from isotropic to polar-dependent cross sections. There are still some discretization errors in these results, but there are apparently no other *significant* errors inherent to the 2D/1D method. These errors could likely be corrected through refinement, but there are not yet any methods for preventing instability as the quadrature and axial mesh are refined (aside from continuing to increase the number of transport sweeps per outer iteration, which is not always sufficient).

Future work will be focused on measures to ensure source positivity *without* significantly compromising the accuracy of the solution so that the mesh can be refined without encountering stability issues, or using a disadvantageously large number of transport sweeps per outer iteration. Given an effective means of ensuring stability for a wider range of problems, we should be able to achieve accuracy close to that of 3D transport with the 2D/1D method.

V. ACKNOWLEDGMENTS

The authors would like to acknowledge Dr. Shane Stimpson of Oak Ridge National Laboratory, whose thesis work advanced the methods in MPACT to the starting point of this work. This work was supported by the Consortium for Advanced Simulation of Light Water Reactors (www.casl.gov), an Energy Innovation Hub (http://www.energy.gov/hubs) for Modeling and Simulation of Nuclear Reactors under U.S. Department of Energy Contract No. DE-AC05-00OR22725.

REFERENCES

1. N. CHO, G. LEE, and C. PARK, "Fusion of Method of Characteristics and Nodal Method for 3-D Whole-Core Transport Calculation," in "Trans. Am. Nucl. Soc.", (2002), vol. 86, p. 322.
2. H. JOO, J. CHO, K. KIM, C. LEE, and S. ZEE, "Methods and Performance of a Three-Dimensional Whole Core Transport Code DeCART," in "Proc. PHYSOR 2004, Chicago, IL, USA," (April 25-29 2004).
3. J. CHO, H. JOO, K. KIM, and S. ZEE, "Three-Dimensional Heterogeneous Whole Core Transport Calculation Employing Planar MOC Solutions," in "Trans. Am. Nucl. Soc.", (2002), vol. 87, pp. 234–236.
4. J. CHO, K. KIM, C. LEE, and H. JOO, "Axial SPN and Radial MOC Coupled Whole Core Transport Calculation," *Nuc. Sci. Tech.*, **44**, 1156–1171 (2007).
5. J. CHO, K. KIM, C. LEE, S. ZEE, and H. JOO, "Axial SPN and Radial MOC Coupled Whole Core Transport Calculation," *J. Nuc. Sci. Tech.*, **44**, 1156–1171 (2007).
6. Y. JUNG and H. JOO, "Decoupled planar MOC solution for dynamic group constant generation in direct three-dimensional core calculations," in "Proc. M&C 2009, Saratoga Srpings, NY, US," (May 3-7 2009), vol. 44.
7. B. KELLEY and E. LARSEN, "2D/1D Approximations to the 3D Neutron Transport Equation. I: Theory," in "Proc. M&C 2013, Sun Valley, ID, USA," (May 5-9, 2013).
8. B. COLLINS, S. STIMPSON, A. GODFREY, B. KOCHUNAS, and T. DOWNAR, "Assessment of the 2D/1D Implementation in MPACT," in "Proc. PHYSOR 2014, Kyoto, Japan," (Sep 28 - Oct 3 2014).
9. T. DOWNAR, B. KOCHUNAS, and B. COLLINS, "Validation and Verification of the MPACT Code," in "Proc. PHYSOR 2016, Sun Valley, ID, USA," (May 1-5 2016).
10. J. ASKEW, "A Characteristics formulation of the Neutron Transport Equation in Complicated Geometry," Tech. Rep. AEEW-M 1108, UKAEA, Winfirth, UK (1972).
11. S. STIMPSON, *An Azimuthal, Fourier Moment-Based Axial S_N Solver for the 2D/1D Scheme*, Ph.D. thesis (2015).
12. S. STIMPSON, B. COLLINS, and T. DOWNAR, "A 2-D/1-D Transverse Leakage Approximation Based on Azimuthal, Fourier Moments," *Nucl. Sci. Eng.*, **185** (2017).
13. M. HURSIN, B. COLLINS, Y. XU, and T. DOWNAR, "The Development and Implementation of a One-Dimensional S_N Method in the 2D-1D Integral Transport Solution," *Nucl. Sci. and Eng.*, **176**, 186–200 (2014).
14. T. ZHANG, E. LEWIS, M. SMITH, W. YANG, and H. WU, "A Variational Nodal Approach to 2D/1D Pin Resolved Neutron Transport for Pressurized Water Reactors," *Nucl. Sci. Eng.*, **186** (2017).
15. B. KELLEY, *An Investigation of 2D/1D Approximations to the 3D Boltzmann Transport Equation*, Ph.D. thesis (2015).
16. N. CHO, G. LEE, and C. PARK, "Refinement of the 2-D/1-D Fusion Method for 3-D Whole-Core Transport Calculation," in "Trans. Am. Nucl. Soc.", (2002), vol. 87, pp. 417–420.
17. G. LEE and N. CHO, "2D/1D Fusion method solutions of the three-dimensional transport OECD benchmark problem C5G7 MOX," *Prog. in Nucl. Energy*, **48**, 410–234 (2006).
18. T. ZHANG, Y. WANG, E. LEWIS, M. SMITH, W. YANG, and H. WU, "Assessment of 2D-Transport/1D-Diffusion Approximations in a Pin Resolved Variational Nodal Method for PWR Calculations," in "these proceedings," (April 16-20 2017).
19. E. LEWIS, M. SMITH, and B. NA, "Benchmark on Deterministic 3-D MOX Fuel Assembly Transport Calculations Without Spatial Homogenization," *Prog. Nucl. Energy*, **48**, 381–382 (2006).
20. F. FINNEMANN and M. WAGNER, "Interface nodal current technique for multi-dimensional reactor calculation," *Atomkernenergie*, **30**, 123 (1977).
21. P. ROMANO, B. HERMAN, N. HORELIK, A. NELSON, B. FORGET, and K. SMITH, "OpenMC: A State-of-the-Art Monte Carlo Code for Research and Development," *Ann. Nucl. Energy*, **82**, 90–97 (2015).
22. T. PANDYA, S. JOHNSON, G. DAVIDSON, T. EVANS, and S. HAMILTON, "SHIFT: A Massively Parallel Monte Carlo Radiation Transport Package," in "Proc. M&C 2015, Nashville, TN, USA," (April 19-23 2015).

APPENDIX

The reference pin powers are compared at 3 uniform planes for both homogenization types (isotropic, polar) for the three cases in Figs. 7–9. The planes are numbered from the bottom. In each case, the isotropic cross section results are shown in the first row, and the polar cross section results are shown on the same scale on the second row. The errors are absolute, compared to a reference solution generated using the Monte Carlo code SHIFT [22]. In all figures, the inner UO_2 assembly is in the bottom left corner. There is a visible improvement apparent in all three cases, which is reflected in the RMS error results given in the main text.

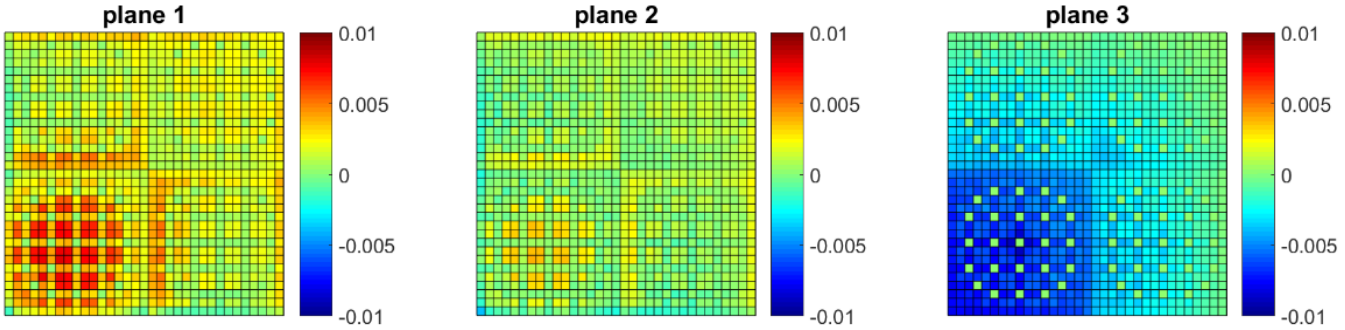

(a) Isotropic XS

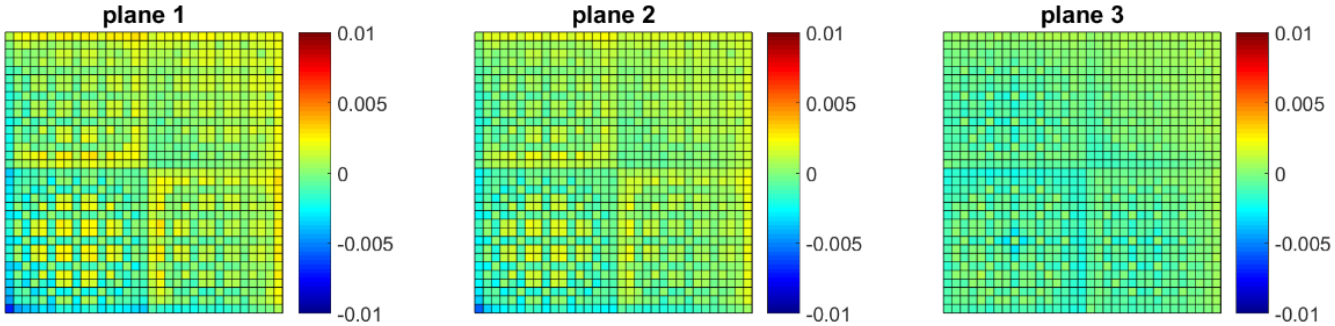

(b) Polar XS

Fig. 7: Pin power errors, C5G7 3D unrodded (first row: isotropic XS, second row: polar XS)

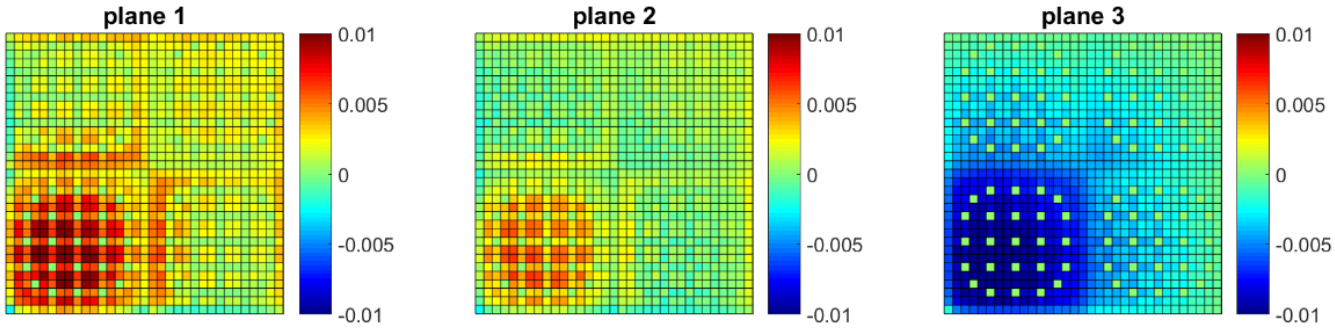

(a) Isotropic XS

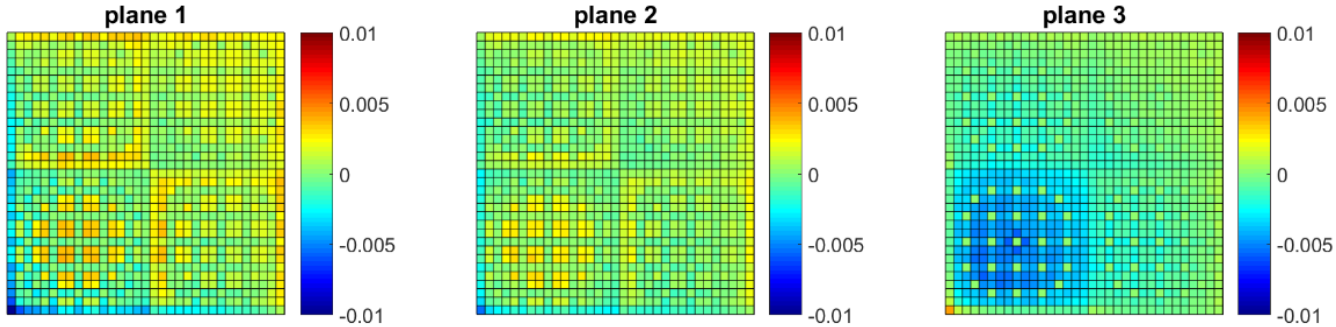

(b) Polar XS

Fig. 8: Pin power errors, C5G7 3D rodded A (first row: isotropic XS, second row: polar XS)

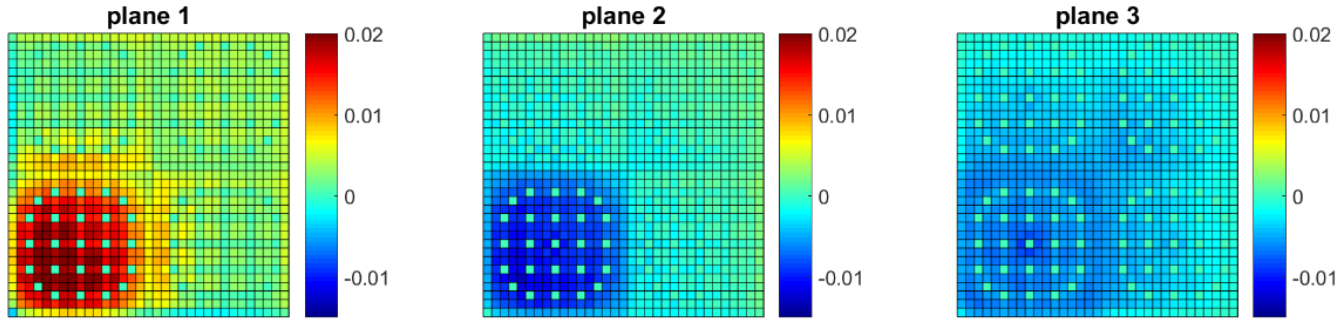

(a) Isotropic XS

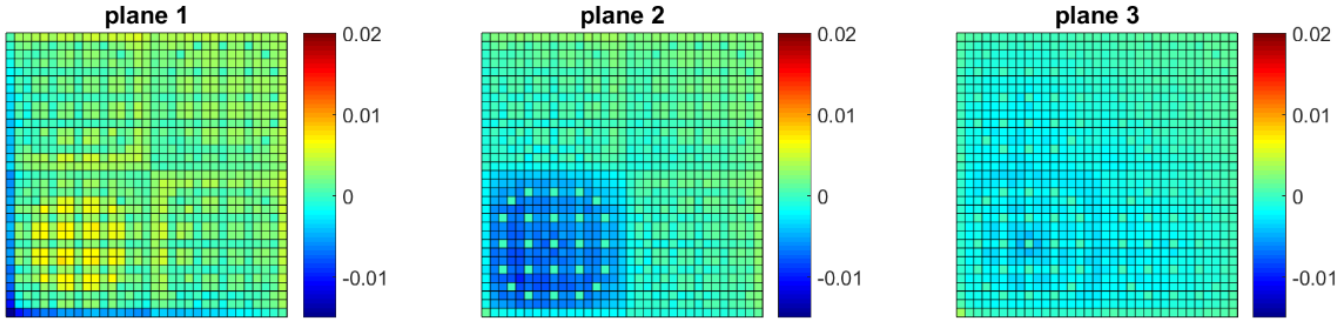

(b) Polar XS

Fig. 9: Pin power errors, C5G7 3D rodded B (first row: isotropic XS, second row: polar XS)